**Luke J. Venstrom**[1]
Department of Mechanical Engineering and Bioengineering,
Valparaiso University,
1900 Chapel Drive,
Valparaiso, IN 46383
e-mail: luke.venstrom@valpo.edu

**Jacob Yager**
Department of Mechanical Engineering and Bioengineering,
Valparaiso University,
1900 Chapel Drive,
Valparaiso, IN 46383
e-mail: jacob.yager@valpo.edu

**Todd Vervynckt**
Department of Mechanical Engineering and Bioengineering,
Valparaiso University,
1900 Chapel Drive,
Valparaiso, IN 46383
e-mail: todd.vervynckt@valpo.edu

**Jonathan D. Ogland-Hand**[2]
Department of Mechanical Engineering and Bioengineering,
Valparaiso University,
1900 Chapel Drive,
Valparaiso, IN 46383
e-mail: johand@ethz.ch

**Shahin S. Nudehi**
Department of Mechanical Engineering and Bioengineering,
Valparaiso University,
1900 Chapel Drive,
Valparaiso, IN 46383
e-mail: shahin.nudehi@valpo.edu

# Measurement of the Natural Convection Heat Transfer in a Magnesium Oxide Electrolytic Cell Concept

*The rate of heat transfer by natural convection between the wall and electrolyte of an electrolytic cell that produces magnesium (Mg) from magnesium oxide (MgO) at temperatures near 1000 °C in a molten fluoride salt electrolyte is presented. An experimental model of the cell was developed that enabled measurements of the heat transfer in the absence of electrolysis and at temperatures less than 100 °C over ranges of Rayleigh numbers from $1 \times 10^{-7}$ to $7 \times 10^{-8}$ and Prandtl numbers from 2 to 6200, ranges that include those anticipated in the operation of the MgO electrolytic cell. The model avoids the substantial experimental challenges associated with the high-temperature, corrosive molten salt to enable a conservative estimate of the heat transfer at a lower cost and greater accuracy than would otherwise be possible. The results are correlated by the expression $Nu = 0.412Ra^{0.23}Pr^{0.15}$ with Nusselt numbers spanning 30–80. The application of the correlation shows that the heat transfer between the cell wall and the molten fluoride electrolyte at ≈1000 °C is characterized by convection coefficients between 100 and 600 W/m$^2$-K and is fast enough to enable heat fluxes up to 10 W/cm$^2$ without compromising the structural integrity of the steel cell wall.* [DOI: 10.1115/1.4046605]

*Keywords: energy efficiency, energy systems, natural and mixed convection*

## Introduction

Magnesium (Mg) is an important commodity in society. It is used as an alloy in the aluminum die-cast industry, as a reactant in steel production, and as a structural metal in several applications, including sporting equipment and automobiles [1]. Magnesium is also energy- and carbon intensive to produce. Depending on the production process, producing 1 kg of magnesium requires up to 133 MJ of energy and leads to the release of up to 26 kg of $CO_2$ [2]. In 2013, the global production of primary magnesium is estimated to have contributed to 0.07% of global $CO_2$ emissions [2]. An energy-efficient and more environmentally friendly approach to Mg production is thus highly desirable [3].

One promising approach is the high-temperature electrolysis of magnesium oxide (MgO). In MgO electrolysis, Mg is produced at atmospheric pressure at temperatures between 930 °C and 1030 °C in an electrochemical reaction driven by an input of electrical energy.

$$MgO(diss) + 0.5C(s) \rightarrow Mg(l) + 0.5CO_2(g) \quad (1)$$

Magnesium oxide is dissolved (diss) in a eutectic mixture of magnesium fluoride and calcium fluoride and electrolyzed with a consumable solid carbon anode to liquid Mg and gaseous carbon dioxide. The carbon dioxide forms at the anode, and the liquid Mg forms at a steel cathode [3]. This process is estimated to require 34 $MJ/kg_{Mg}$ of energy or less depending on whether it incorporates a solar thermal energy input [4]. Furthermore, $CO_2$ emissions are estimated at $< 5 kg_{CO_2}/kg_{Mg}$ [4].

In addition to reducing overall energy requirements and lowering $CO_2$ emissions, one of the potential advantages of MgO electrolysis is that it allows some of the energy required for Mg production to be provided in the form of high-temperature process heat. The total energy required for the process is the change in enthalpy required to heat the reactants to the operational temperature, drive the endothermic reaction, and flash vaporize the liquid magnesium as a means to recover it (Fig. 1). Of the total energy required, at least an amount equal to the change in the Gibbs free energy must be supplied as electric energy. The remaining amount may be supplied as thermal energy. Reaction kinetics and Ohmic resistance require that more than the thermodynamic minimum amount of electric energy be added (the overvoltage), but an analysis of the MgO electrochemistry suggests that 30% of the energy required to produce Mg from MgO could be thermal energy [3]. No industrial electrolytic process, to our knowledge, takes advantage of the opportunity to substitute thermodynamically valuable electric energy with thermal energy but doing so promises to lower operating costs,

[1]Corresponding author.
[2]Present address: Geothermal Energy and Geofluids Group, Department of Earth Sciences, ETH-Zürich, Sonneggstrasse 5, 8092 Zürich, Switzerland.

Manuscript received December 27, 2019; final manuscript received March 1, 2020; published online March 6, 2020. Assoc. Editor: Aaron P. Wemhoff.

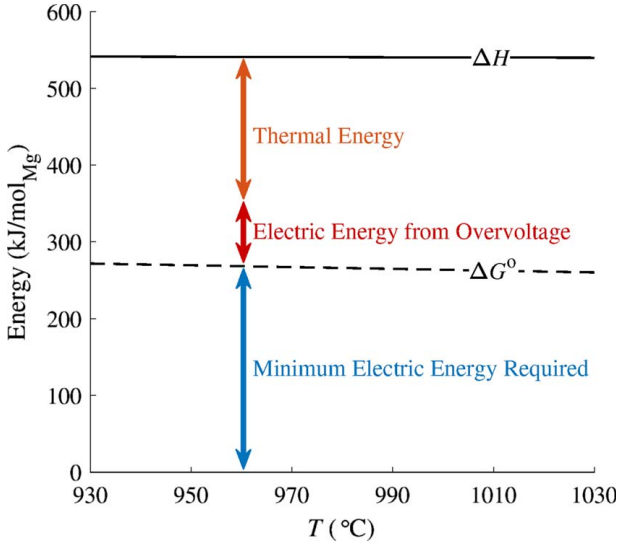


**Fig. 1 The total energy required in the MgO electrolytic process as defined by the total change in enthalpy ($\Delta H$) and the minimum electric energy input required as defined by the change in the Gibbs free energy of Eq. (1) ($\Delta G°$)**

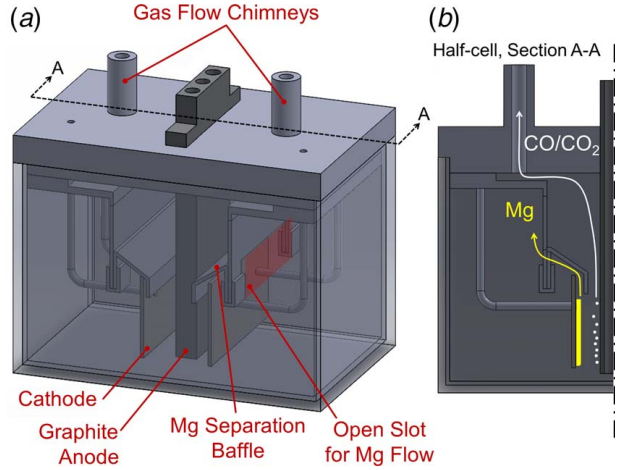


**Fig. 2 Sketch of the electrochemical cell design concept: (*a*) an isometric view with transparent cell walls to expose the internal electrodes and baffles and (*b*) a section view of half of the cell depicting the flow paths of the reaction products**

reduce emissions, or both. If the thermal energy were to be supplied via concentrated sunlight, fuel costs and their associated carbon emissions are avoided entirely. Alternatively, if the thermal energy is supplied via the combustion of natural gas, fuel costs could be reduced so long as natural gas remains cheaper than grid-purchased electricity [5].

When thermal energy is substituted for electric energy in MgO electrolysis, heat must transfer through the interface between the electrolytic cell wall and the molten fluoride electrolyte. If the heat transfer through the interface is not fast enough, the cell wall will overheat and melt, leading to catastrophic process failure. For example, the maximum operating temperature of 310 grade stainless steel is ca. 1100 °C [6]. If the cell wall is constructed from 310 stainless steel and the cell temperature is 930 °C, the maximum allowable temperature difference between the cell wall and the electrolyte is $\Delta T = 170$ °C. With concentrated solar radiation, heat fluxes of 10 W/cm$^2$ are possible [7] so that the heat transfer coefficient between the cell wall and the electrolyte must be at least 590 W/m$^2$-K to ensure $\Delta T \leq 170$ °C. The question becomes whether such a heat transfer coefficient can be realized via natural convection because actively pumping or stirring molten fluorides to provide forced convection would add significant complexity and cost to the cell.

In this paper, we answer this question for one promising MgO electrolytic cell concept developed at Valparaiso University [3]. We begin by reviewing the concept for the electrolytic cell which has been reported on previously [8]. We then describe the approach developed to measure the rate of heat transfer in a low-temperature experimental model of the MgO electrolytic cell. This approach avoids the substantial experimental challenges and costs associated with measuring temperature in a high-temperature system filled with corrosive molten salts and enables the use of an automatically controlled guard heater for accurate control of the applied heat flux. A similar approach could be applied to estimate the rate of convection heat transfer in other high-temperature molten salt systems such as molten salt thermal storage or ZnO electrolysis. Finally, the results are presented, and a correlation for the rate of natural convection heat transfer is developed and used to estimate the rate of heat transfer in the MgO electrolytic cell concept.

## Electrolytic Cell Concept

A sketch of a design concept for the MgO electrolytic cell first described in Ref. [3] is provided in Fig. 2. It consists of a single rectangular graphite anode from which $CO_2$ evolves at the cell midplane, two cathodes from which liquid Mg evolves on either side of the anode, and separation baffles located above the cathodes. This concept addresses two challenges of producing Mg from MgO electrolytically. First, the electrochemical reaction products, liquid Mg and gaseous $CO_2$, are separated to prevent their back-reaction. Reaction products are separated using the baffles, which can be seen in the isometric view of the cell in which the cell walls have been made intentionally transparent (Fig. 2(*a*)). As the buoyant bubbles of gaseous $CO_2$ and liquid Mg rise to the top of the electrolyte, the Mg bubbles are directed to a chamber isolated from the $CO_2$ through a slot (shaded region in Fig. 2(*a*)). The anticipated flow path of the reaction products is depicted in Fig. 2(*b*). Second, the cell concept allows for the unobstructed charge flow between the cathode and anode surfaces which are in close proximity to one another, minimizing Ohmic losses that decrease the amount of thermal energy that can be used for Mg production. The cathode–anode gap is two to three times smaller than the gap in Hall-Héroult cells [9].

The MgO electrolytic cell could be heated through the side walls, the bottom wall, or a combination of both. If the cell is heated via concentrated sunlight, however, heating would likely occur from the bottom. We refer the reader to Ref. [4] for a detailed description of how the MgO electrolytic cell could be heated with concentrated sunlight using an active-reflux sodium heat pipe receiver. In brief, sodium is evaporated in a solar power tower and transported to the MgO electrolytic cell where it condenses, releasing the latent energy of condensation in a heat exchange unit at the bottom of the cell. In this case, convection heat transfer between the bottom wall and the electrolyte will depend on the magnitude of the imposed temperature gradient, the geometry of the enclosure, and the properties of the electrolyte [10,11]. Convection only occurs if the heating is strong enough to generate buoyant forces via temperature gradients in the fluid that are large enough to overcome the viscous forces that resist fluid motion. The onset of convection is characterized by a critical value of the Rayleigh number where the Rayleigh number is defined as

$$\mathrm{Ra} = \frac{g\beta\Delta T H^3}{\alpha\nu} \tag{2}$$

In rectangular enclosures *without* internal surfaces like the baffles and electrodes of the MgO electrolytic cell, convection begins at a Rayleigh number between $1.7 \times 10^3$ and $2.0 \times 10^4$ for enclosures with height-to-width ratios between 0 and 2, respectively [11]. (The height-to-width ratio of the MgO electrolytic cell concept is

approximately 1.0.) The baffles and electrodes in the MgO electrolytic cell introduce additional resistance to fluid motion such that an even larger Rayleigh number may be required to initiate convection. Furthermore, after the initiation of convection, internal surfaces are known to suppress the strength of natural convection [11,12]. Thus, correlations for calculating the heat transfer coefficient based on heat transfer measurements in empty enclosures are not applicable. In order to characterize the natural convection heat transfer in the MgO electrolytic cell, it must be measured.

## Methodology

**Experimental Approach.** A direct measurement of the convection coefficient during MgO electrolysis in the molten fluoride electrolyte, while preferred, presents substantial experimental challenges due to the corrosiveness of the molten fluorides, the solid-to-liquid phase change upon heating and cooling, operating temperatures of ≥930 °C, and convoluting effects from electric currents. In an effort to increase the accuracy of the heat transfer measurement in the face of these challenges and to reduce the cost, we created an experimental model of the MgO electrolytic cell concept that uses low-temperature, non-corrosive fluids. Similar experimental models have been adopted to study mass and heat transfer in $MgCl_2$ electrolysis [13,14].

The use of a low-temperature experimental model ($T < 100$ °C) to estimate the convection heat transfer in a high-temperature system containing molten fluorides ($T > 900$ °C) offers several advantages that are not unique to the MgO electrolysis process of the present study. First, high-accuracy temperature sensors can be employed to measure temperature, and these sensors can be accurately located within the system prior to heating. (Accurate thermocouple placement in molten salts is difficult because the salts are solid at room temperature.) Additionally, surface-mounted electric heaters can be used to apply accurate heat fluxes to the cell via the application of guard heaters to minimize heat loss. Finally, the cost of the measurement is substantially reduced because high-temperature, corrosion-resistant materials are not required. By employing an approach similar to the one developed in the present study, scientists and engineers studying convection heat transfer in other molten salt systems, such as electrolytic Zn or Al production and molten salt thermal storage systems for concentrated solar power, could also realize these advantages.

The use of an experimental model requires that natural convection in the model is similar to the natural convection in the real system. The key similarity parameters for natural convection heat transfer are the Nusselt number, the Rayleigh number, and the Prandtl number. Geometry (baffle-channel placement, cathode-anode gap size, height-to-width ratio, etc.) is also a critical factor in determining the heat transfer but is fixed in the present study to be geometrically similar to the cell concept of Fig. 2.

The relative strength of the heat transfer is characterized by the Nusselt number, defined in the present study as

$$\mathrm{Nu} = \frac{q''}{\bar{T}_w - \bar{T}_f}\frac{H_f}{k_f} \tag{3}$$

The Nusselt number is a function of the Rayleigh number (Eq. (2)) and, to a lesser extent, the Prandtl number. The Prandtl number is defined as the ratio of the kinematic viscosity and the thermal diffusivity of the fluid.

$$\mathrm{Pr} = \frac{\nu}{\alpha} \tag{4}$$

The Rayleigh number and Prandtl number capture the impact of fluid motion on the natural convection heat transfer.

To demonstrate that similarity is attained between the MgO electrolytic cell concept and an experimental model using non-corrosive fluids at lower temperatures, consider the following example. The cell of Fig. 2 is filled to a height of 10 cm with a eutectic mixture of $MgF_2$ and $CaF_2$ at 930 °C. At the maximum allowable temperature difference between the cell wall and the fluid of $\Delta T = 170$ °C, the Rayleigh number is $1.6 \times 10^9$. Similar Rayleigh numbers are achieved using, e.g., water, but at lower temperatures. In water at the same height of 10 cm and at 50 °C, the temperature difference to achieve the same Rayleigh number of $1.6 \times 10^9$ is $\Delta T = 28.6$ °C, a value that is physically attainable and measureable in the laboratory.

Potential limitations of the low-temperature model approach to studying heat transfer in the electrolytic cell concept include differences in the Prandtl numbers of the model electrolytes and molten fluorides and differing temperature dependencies of the fluid properties. To address these limitations, we measured the heat transfer in three model electrolytes: water, oil, and ethylene glycol. Due to the temperature dependence of the properties of these fluids, the rate of heat transfer is measured for Prandtl numbers from 2 to 6200. The low range of the Prandtl numbers is resolved in the water system, the intermediate range of the Prandtl numbers is resolved in the ethylene glycol system, and the high range of the Prandtl numbers is resolved in the oil system. The Prandtl numbers expected in the $MgF_2$–$CaF_2$ molten fluoride electrolyte fall in the range 5–9 [15].

The low-temperature model approach also neglects radiation heat transfer, the presence of multiple gas and liquid phases in the electrolyte, and any effects of electrolysis on fluid motion. Due to the buoyancy of the $CO_2$ and Mg(l), these phases will be concentrated in the area next to the electrodes where they are evolved and near the top of the cell where they are extracted, and thus likely have a minimal impact on the heat transfer at the bottom of the cell. Furthermore, heat transfer should be conservatively measured without radiation heat transfer and electrolysis: with $CO_2$ and liquid Mg rising at the electrode surfaces during electrolysis and the endothermic reaction energy sink, electrolyte circulation will be augmented beyond what is achieved with natural convection driven by external heating alone. For example, it has been shown in a numerical study that the more rapid the electrolysis in a $MgCl_2$ electrolytic cell that also produces buoyant gas and liquid reaction products, the more rapid heat transfer is in the cell [16]. Since the objective in the present study is determine whether heat transfer is sufficiently fast to permit heating from an external source through the bottom wall of the MgO electrolytic cell concept, a conservative measure of the heat transfer, i.e., one that represents the lower bound of what is possible, is sufficient.

**Experimental Setup.** Two-dimensional section views of the experimental model used to measure the natural convection heat transfer in the electrolytic cell concept (Fig. 2) are shown in Fig. 3. The experimental model consists of a smaller, but geometrically similar, mockup of the MgO electrolytic cell filled with a model fluid and covered with a water-cooled lid that is placed on a heating system and surrounded by insulation. The experimental model is made level using an aluminum base with adjustable feet. Contact resistance between the heating system and the model cell is reduced by squeezing the model cell and the heating system together using rods and nuts evenly spaced around the perimeter of the cell and threaded into the aluminum base. Contact resistance is further reduced with the application of thermally conductive paste at the interface between the heating system and the model cell.

The model cell is 152.4 mm wide, 101.6 mm deep, and 101.6 mm tall (height-to-width ratios of 0.7 and 1.0, respectively) with 3.2-mm-thick steel walls. In all experiments, the cell was filled with fluid to a height of $H_f = 98$ mm. A 3D printer was used to fabricate geometrically similar versions of the electrodes and separation baffles of the cell. The 3D printer ensured accurate reproduction of the size of, and spacing between, the internal surfaces of the cell, but produced plastic versions of the components with a lower thermal conductivity than those in the real cell made of steel and carbon. The thermal conductivity mismatch is expected to have a minimal impact on the heat transfer coefficient between the cell wall and fluid because the sizes of the baffles and electrodes are small relative to the size of the cell [17]. The locations of the

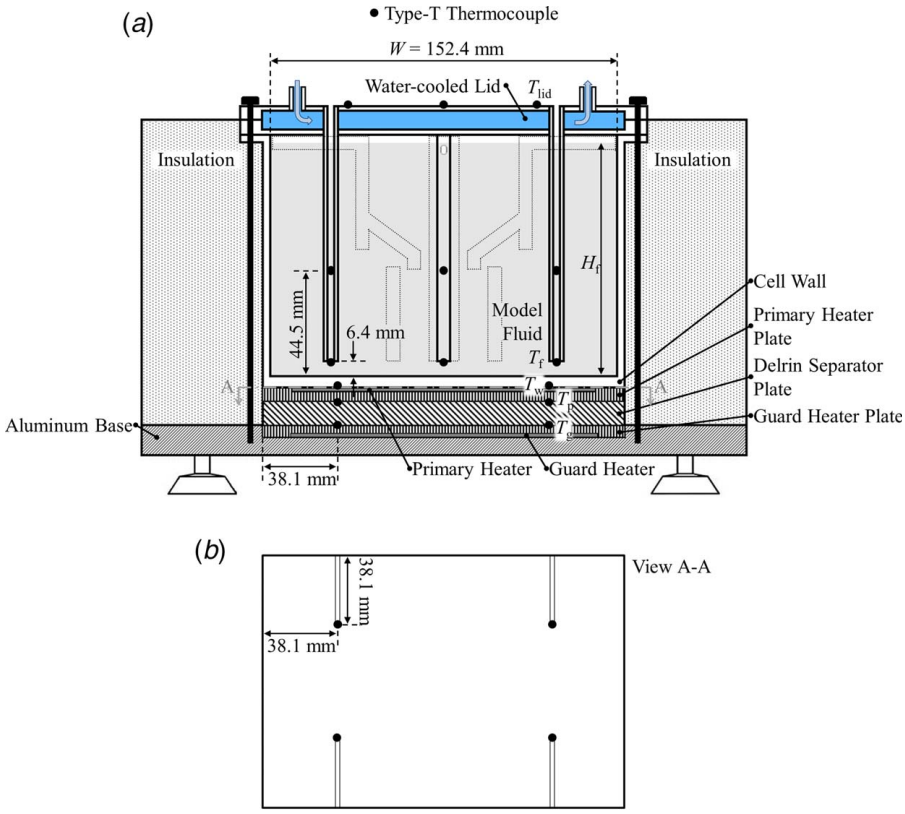


**Fig. 3 (*a*) Vertical section view of the experimental model used to measure the heat transfer in the MgO electrolytic cell concept of Fig. 2. The position of the baffle and electrode surfaces are indicated by the dashed lines. (*b*) Horizontal section view A-A of the cell wall. In both (*a*) and (*b*), black dots denote the locations of thermocouple junctions.**

electrode and separation baffle surfaces in the experimental model are indicated by dashed lines in Fig. 3(*a*).

The model cell is heated from below using an electric, automatically controlled heating system. The system consists of a thin primary heater separated from a guard heater by a 25.4-mm-thick polyoxymethylene (Delrin) plate. Both the primary heater and the guard heater are embedded into 3.2-mm-thick copper plates to minimize temperature variation over the heater surfaces. The heating system directs as much of the primary heater power to the model cell as possible by minimizing the heat loss from the primary heater to the surroundings through its bottom face. Heat loss through the bottom face is minimized by adjusting the guard heater power until the temperature difference across the Delrin separator plate is zero within the practical limits imposed by measurement accuracy and the controller. Heat loss through the sides of the primary heater is negligible due to the insulation there and the thinness of the heater plate which reduces the area for heat loss.

To control the guard heater, we developed a proportional plus integral (PI) controller. The feedback signal for the controller is the difference between the spatially averaged temperatures of the primary heater and guard heater plates, and the control signal is the guard heater power. The proportional and integral gains of the controller were selected using simulations to be 50 and 1, respectively. These values mitigate ringing while also providing a sufficiently rapid response. The difference in the plate temperatures approaches zero in 2–3 min. The model used to simulate the controller and select the gains is presented in Ref. [18] as well as a proof that the control system is globally stable.

Throughout an experiment, a flow of tap water was maintained in the lid of the model cell. Actively cooling the cell lid was required to establish a measureable temperature difference between the fluid and the cell wall. Without the cooling, the resistance to heat transfer through the top of the cell was large relative to the resistance to heat transfer through the bottom of the cell such that most of the temperature drop for heat transfer occurred between the cell lid and the surrounding air. Actively cooling the lid reduced the resistance to heat transfer through the top of the cell, increasing the temperature difference between the cell wall and the fluid to measureable levels.

The temperatures of the primary heater plate, guard heater plate, cell wall, fluid, and cell lid were measured with small diameter copper-constantan thermocouples (type T, 30 gauge wire). Within the fluid of the model cell, small diameter, hollow aluminum tubing was used to precisely locate the thermocouple junctions 6.4 mm and 44.5 mm away from the cell wall at five different locations in the horizontal plane, the plane normal to the direction of heat transfer. Thermocouples were embedded into the cell wall with thermally conductive epoxy at the same locations in the horizontal plane as in the fluid region. Four thermocouples were positioned at a distance equal to one-fourth of the side of the heated area from the corners of the copper plates in accordance with ASTM test standard C177-13 (see Fig. 3(*b*)). These thermocouples were also secured into position with thermally conductive epoxy. Variations in temperature in the direction normal to heat transfer were small, typically less than 1 °C. All temperature measurements made in the same horizontal plane were thus averaged for application in the calculation of the heat transfer parameters.

**Data Reduction.** At steady-state with a negligible temperature gradient across the Delrin separator plate, the convection coefficient associated with the natural convection heat transfer between the cell wall and the fluid is calculated using temporally and spatially

averaged temperatures as

$$h_f = \frac{q_p}{A_c(\bar{T}_w - \bar{T}_f)} \tag{5}$$

The primary heater power, $q_p$, was quantified as the quotient of the square of the heater voltage and the electrical resistance of the heater. The electrical resistance of the heater was measured using an Ohmmeter prior to the execution of each experiment. To confirm that the heater resistance change upon heating was negligibly small, the power to the heater was temporarily disconnected in one experiment, while the system was at temperature and the heater resistance measured. It increased by less than 0.1%.

The Rayleigh number and the Nusselt number are calculated at steady-state according to their definitions in Eqs. (2) and (3), respectively. For the Rayleigh number, the temperature difference is calculated as $\Delta T = \bar{T}_w - \bar{T}_f$, and all fluid properties are evaluated at the mean temperature $T_m = 0.5(\bar{T}_w + \bar{T}_f)$. The properties for water, ethylene glycol, and oil were taken from Ref. [10].

Measurement uncertainty was analyzed based on the recommendations in Refs. [19,20]. Elemental errors in measured variables are combined using the Kline–McClintock method and propagated to the parameters (e.g., the Rayleigh number) using the sequential perturbation method. The dominant source of uncertainty in the experiments was determined to be the measurement of temperature. We thus describe how we estimated precision and systematic uncertainty in the temperature measurements.

*Precision Uncertainty.* The temperatures of the guard heater, primary heater, cell wall, fluid, and cell lid were measured at multiple locations in planes perpendicular to the direction of heat transfer (Fig. 3(*b*)) at steady-state conditions over a period of at least 30 min at a sampling rate of 0.1 Hz. Variations in temperature in the direction normal to the direction of heat transfer were always <1 °C. These small variations were thus included in the precision error estimate. Two sources of precision error are thus accounted for using pooled statistics [19]: unsteadiness and spatial nonuniformity in the direction normal to heat transfer. A typical value for the precision uncertainty was ±0.5 °C at a 95% confidence interval.

*Systematic Uncertainty.* An estimate of the range of bias error in the measurements of temperature was determined via an end-to-end calibration of the T-type thermocouple circuits and the National Instruments data acquisition system used to read and display their output over the temperature range from 20 °C to 100 °C. Class 1/10 DIN platinum resistance temperature detectors (RTDs) paired with a high-accuracy Isotech TTI-10 ohmmeter and a constant temperature circulating water bath served as the standard in the calibration experiment. The uncertainty in the RTD-ohmmeter temperature-measurement system was ±0.05 °C as reported by the manufacturer. The uncertainty associated with spatial variations of temperature in the water bath was estimated as the maximum temperature difference between two RTDs spatially separated in the water bath to be 0.05 °C. Based on the calibration, systematic uncertainty in the temperature measurements is ≤0.1 °C over the range 20–100 °C.

## Results and Discussion

Figure 4 shows the output of a typical experiment with oil as the model fluid. Similar trends are observed in the results with water and ethylene glycol. In the figure, the spatially averaged temperatures of the guard heater plate, the primary heater plate, the cell wall, the oil, and the lid are plotted over time along with the applied heat flux. The cell is subjected to 16 increasing levels of heat flux between 0.37 kW/m$^2$ and 3.24 kW/m$^2$ by increasing the primary heater voltage every 3 h. Upon the application of each new level of heat flux, the temperatures of the heater plates, the cell wall, and the fluid initially rise rapidly. The rate of increase slows as the system approaches a new thermal equilibrium. Temperatures change by less than 0.1 °C in a 30 min period (<0.2 °C/s) before the heat flux increases again. The temperature of the water-cooled lid, on average, slowly increases from 23.5 °C to 30.5 °C during the two-day experiment. The cell lid also experiences small fluctuations in temperature on an order of 1 °C that correlate to the on–off operation of the heat pump unit controlling the laboratory ambient air temperature.

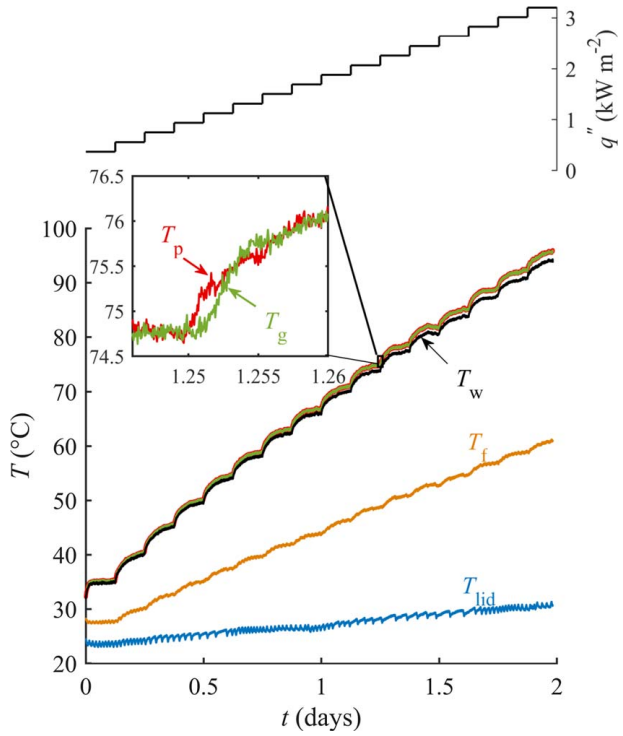


**Fig. 4 The spatially averaged temperatures of the primary heater plate, guard heater plate, cell wall, fluid, and cell lid and the applied heat flux measured for the cell filled with oil. The inset zooms in on the primary and guard heater plate temperatures after the heat flux is increased at $t = 1.25$ days.**

The data in Fig. 4 demonstrate the success of the PI control of the guard heater. The controller was able to adjust the guard heater power to effectively eliminate the steady-state difference in the temperature between the primary and guard heater plates. The average difference in the plate temperatures during steady-state periods is ≤0.05 °C with a standard deviation of ≤0.09 °C. Even during transients, the controller maintained a temperature difference under 0.7 °C. An example of the small temperature differences observed between the primary and guard heater plate during the transients is depicted in the inset of Fig. 4, which shows the primary and guard heater plate temperatures for the first 15 min after the heat flux was increased from 2.07 kW/m$^2$ to 2.26 kW/m$^2$ at $t = 1.25$ days.

As the heat flux increases so do differences in temperature between the cell components. The difference between the cell wall temperature and oil temperature increases from 7.3 °C at the lowest heat flux to 34.7 °C at the highest flux (Fig. 4). It is this temperature difference that characterizes the resistance to heat transfer between the cell wall and the fluid and it is thus used to calculate the Nusselt number (Eq. (3)) and Rayleigh number (Eq. (2)) for the steady operation.

The Nusselt number at steady-state measured for the oil, ethylene glycol, and water is shown in Fig. 5(*a*) as a function of the Rayleigh number. The corresponding Prandtl number of the fluid at each measurement point is provided in Fig. 5(*b*). Measurement uncertainty is indicated in the figure by the vertical bars. (For clarity, the uncertainty is only shown at a datum for each fluid system.) For Rayleigh numbers between $1.0 \times 10^6$ and $6.6 \times 10^8$, Nusselt

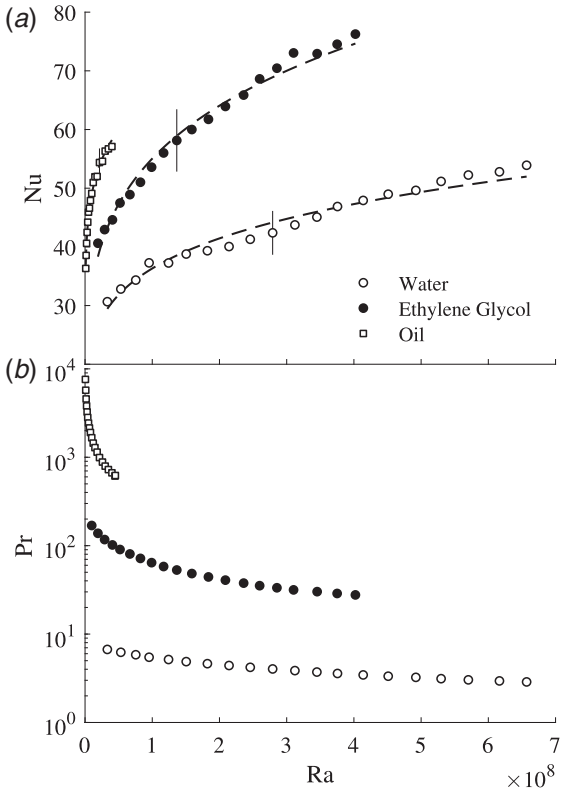


**Fig. 5 (*a*) The Nusselt number measured for natural convection heat transfer in the model electrolytic cell in water, ethylene glycol, and oil and (*b*) the corresponding Prandtl number of the fluid. Measurement uncertainty is indicated by the vertical bars; dashed lines are present to help guide the eyes.**

numbers range from 30 to 80, indicating the enhancement of heat transfer by bulk motion of fluid in the cell. The critical Rayleigh number for fluid motion in the cell was thus exceeded for all conditions considered in the present study, and it can be inferred that the critical Rayleigh number for the cell lies between $\approx 2.0 \times 10^4$, the value for an enclosure without internal surfaces [11], and $1.0 \times 10^6$, the lowest value at which data are available, even though the exact value was not resolved. Furthermore, the Nusselt number, interpreted as a dimensionless temperature gradient at the cell wall, increases with the Prandtl number as expected due to the growing difference in the thicknesses of the velocity and thermal boundary layers. At a Rayleigh number of $0.3 \times 10^8$, the Nusselt number is 56, 43, and 30 for heat transfer in the oil, ethylene glycol, and water, respectively, with Prandtl numbers of 794, 117, and 7, respectively.

To allow the heat transfer data in Fig. 5 to be extrapolated to the MgO electrolytic cell concept filled with molten fluoride salt, the data were fit to an equation of the form

$$\mathrm{Nu} = C\mathrm{Ra}^n\mathrm{Pr}^m \tag{6}$$

where $C$, $n$, and $m$ are constants and fluid properties are evaluated at the film temperature $T_m$. This form was chosen due to its similarity to the form of the correlation suggested for enclosures heated from below without internal surfaces [21], the problem bearing the closest resemblance to the MgO electrolytic system of the present study. Furthermore, the correlation of Eq. (6) provided a statistically significant better fit to the data with an adjusted $R^2_{\mathrm{adj}}$ of 0.94 than alternative correlations considered, including the mathematically simpler $\mathrm{Nu} = C\mathrm{Ra}^n$ ($R^2_{\mathrm{adj}} = 0.15$). Using least-squares regression, $C$, $n$, and $m$ in Eq. (6) were determined to be 0.4116, 0.23, and 0.15, respectively. Figure 6 shows the heat transfer correlation and the uncertainty in the correlation at a 95% confidence interval.

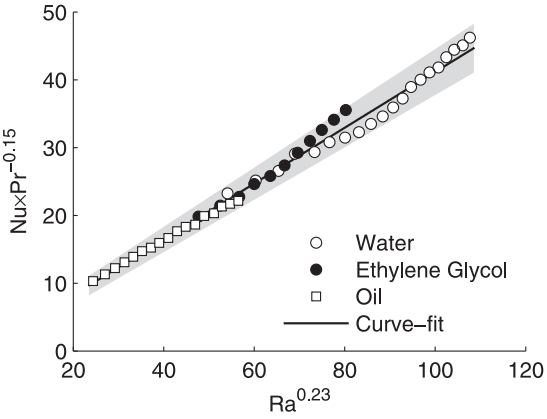


**Fig. 6 The correlation for natural convection heat transfer in the baffle-channel cell concept. The shaded region depicts the uncertainty associated with the correlation.**

The uncertainty is depicted by the shaded region in the figure. It is less than ±20% of the Nusselt number.

Using the correlation, the heat transfer measured in the low-temperature model is extrapolated to estimate the range of heat transfer coefficients and heat fluxes in the MgO electrolytic cell concept as a function of the temperature difference between the electrolytic cell wall and the molten fluoride at an assumed cell operating temperature of 930 °C (Fig. 7). Temperature differences at the cell wall–fluid interface up to 170 °C are included because this is the operating range for which steel can be safely used as the cell wall containing material. Doing so, however, requires that the correlation be extended slightly beyond the range of Rayleigh numbers for which data were collected in the experimental model. In the MgO electrolytic cell, Rayleigh numbers up to $30 \times 10^8$ are estimated at the highest rates of heat transfer (see the second abscissa axis in Fig. 7), whereas data were collected up to $0.7 \times 10^8$. In addition, we show the extrapolation for cryolite ($Na_3AlF_6$) because the temperature dependence of the density is not available for the $MgF_2$–$CaF_2$ electrolyte: the properties of cryolite serve as a suitable proxy for the properties of $MgF_2$–$CaF_2$ since both fluids are molten fluorides. For reference, we provide in Table 1 representative values of the thermophysical properties of cryolite at 1000 °C and,

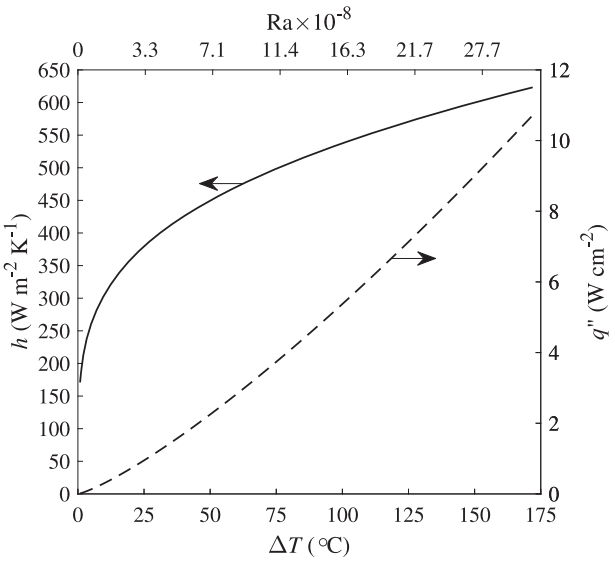


**Fig. 7 Estimate of the heat transfer coefficient and corresponding cell wall heat flux for the MgO electrolytic cell concept over the range of permissible temperature differences to prevent cell wall failure**

**Table 1 Thermophysical properties of cryolite, the molten fluoride used as a proxy for the $MgF_2$–$CaF_2$ electrolyte, and, when data are available, for the $MgF_2$–$CaF_2$ electrolyte at 1000 °C**

| Property | Cryolite | $MgF_2$–$CaF_2$ electrolyte |
|---|---|---|
| Density, $\rho$ (kg/m$^3$) | 2095 | 2687 |
| Coefficient of thermal expansion, $\beta$ (K$^{-1}$) | $4.5\times10^{-4}$ | – |
| Thermal diffusivity, $\alpha$ (m$^2$/s) | $2.6\times10^{-7}$ | – |
| Kinematic viscosity, $\nu$ (m$^2$/s) | $1.33\times10^{-6}$ | $2.8\times10^{-6}$ |
| Thermal conductivity, $k_f$ (W/m-K) | 0.79 | – |
| Prandtl number, Pr | 5.1 | – |

when available, the $MgF_2$–$CaF_2$ electrolyte. Properties for cryolite are from Ref. [9] and properties for the $MgF_2$–$CaF_2$ electrolyte are from Ref. [15].

The extrapolation confirms that the natural convection heat transfer coefficient in the electrolytic cell concept is fast enough to allow for an externally delivered solar (or natural gas) thermal input. The heat transfer coefficient at the interface between the cell wall and the molten fluoride electrolyte is greater than 200 W/m$^2$-K when the temperature difference between the cell wall and the electrolyte is greater than 10 °C. At a temperature difference of $\Delta T = 170$ °C, the heat transfer coefficient is estimated to be 598 W/m$^2$-K, large enough to permit a heat transfer input at a flux up to 10 W/cm$^2$ that could be delivered from concentrated solar radiation [7].

## Summary and Conclusions

In this paper, we present a technique to measure the natural convection heat transfer in a promising MgO electrochemical cell concept that operates at ≈1000 °C using a molten fluoride salt electrolyte but at significantly lower temperatures in an experimental model. The technique presented avoids the substantial experimental challenges associated with the corrosiveness of the molten fluoride, the solid-to-liquid phase change upon heating and cooling, and extreme temperatures, and enables a conservative measurement of the heat transfer at a lower cost and greater accuracy than would be possible in the extreme environment of the real system. Low cost and improved accuracy are achieved because the low-temperature experimental model is built from common materials and uses instrumentation capable of accurate measurements that would otherwise be destroyed at the extreme temperatures in the real system. For example, the model included an automatically controlled guard heater to control heat loss from a primary heater, both comprised of surface-mounted electric heaters, and thereby enable accurate measurements of the heat flux into the model electrolytic cell. Water, ethylene glycol, and oil—non-corrosive fluids—were used as model fluids for the corrosive, high-temperature molten fluoride electrolyte used for MgO production. The technique could be adapted to study the heat transfer in other high-temperature, molten salt-based systems.

The convection coefficient for the heat transfer between the wall of the cell and the fluid was measured for Rayleigh numbers in the range $1\times10^5$–$7\times10^8$ and Prandtl numbers in the range 2–6200. The corresponding Nusselt numbers ranged from 30 to 80, indicating an enhancement in the heat transfer at the cell wall–fluid interface due to fluid motion. The experimental results suggest that the heat transfer coefficient in the MgO electrolytic cell filled with a eutectic mixture of $MgF_2$ and $CaF_2$ will be in the 200–600 W/m$^2$-K range for heat fluxes spanning 1–10 W/cm$^2$. The heat transfer is fast enough to limit the cell wall temperature to within the working temperature limits of steel, permitting the cell to be heated with concentrated solar radiation.

## Acknowledgment

We are grateful to the U.S. Department of Energy ARPA-E program for financial support for this work under the cooperative agreement DE-AR0000421. We also thank Patrick O'Neil, Ryan Hall, and Kent Warren for their contributions in fabricating and calibrating thermocouples.

## Nomenclature

$g$ = gravitational acceleration constant
$h$ = convection heat transfer coefficient
$k$ = thermal conductivity
$m$ = constant in empirical correlation
$n$ = constant in empirical correlation
$q$ = rate of heat or energy transfer
$t$ = time
$C$ = constant in empirical correlation
$H$ = height of the fluid layer
$L$ = separator plate thickness
$T$ = temperature
$W$ = width of the fluid layer
$\bar{T}$ = temperature spatially averaged along a plane normal to the direction of heat transfer
$q''$ = heat flux Rayleigh number, $g\beta(T_w - T_f)H_f^3\alpha^{-1}\nu^{-1}$
$A_c$ = area normal to the direction of heat transfer
Nu = Nusselt number, $h_f H_f k_f^{-1}$
Pr = Prandtl number, $\nu\alpha^{-1}$
$\alpha$ = thermal diffusivity
$\beta$ = coefficient of thermal expansion
$\nu$ = kinematic viscosity
$\Delta G^o$ = change in Gibbs free energy change with reactants in standard states
$\Delta H$ = enthalpy change of the process
$\Delta T$ = temperature difference

### Subscripts

f = fluid layer
g = guard heater or guard heater copper plate
p = primary heater or primary heater copper plate
s = separator plate wCell wall
lid = cell lid
∞ = surroundings

## References

[1] Cole, G. S., 2016, "Summary of "Magnesium Vision 2020: A North American Automotive Strategic Vision for Magnesium"," *Essential Readings in Magnesium Technology*, S. N. Mathaudhu, A. A. Luo, N. R. Neelameggham, E. A. Nyberg, and W. H. Sillekens, eds., Springer, Cham, New York, pp. 35–40.
[2] Ehrenberger, S., 2013, *Life Cycle Assessment of Magnesium Components in Vehicle*, International Magnesium Association, Wauconda, IL.
[3] Palumbo, R., Korenko, M., Larson, C., Venstrom, L., Duncan, S., Nudehi, S., Schoer, J., Toberman, J., Prusinksi, W., Johnson, D., Robbinson, B., Barkely, S., Warren, K., Diver, R., Šimko, F., and Boča, M., 2015, "Thermal Electrolytic Production of Mg from MgO: Reflections on Commercial Viability," *Magnesium Technology 2015*, M. V. Manuel, A. Singh, M. Alderman, and N. R. Neelameggham, eds., Springer, Cham, New York, pp. 43–48.
[4] Korenko, M., Larson, C., Blood, K., Palumbo, R., Nudehi, S., Diver, R., Blood, D., Šimko, F., and Venstrom, L. J., 2017, "Technical and Economic Evaluation of a Solar Thermal MgO Electrolysis Process for Magnesium Production," Energy, **135**, pp. 182–194.
[5] Enkvist, P., Naucler, T., and Rosander, J., 2007, "A Cost Curve for Greenhouse Gas Reduction," McKinsey Q., **1**, p. 34.
[6] Davis, J. R., 1994, Stainless Steels, ASM International, Maryland Park, OH, pp. 505–525.
[7] Li, X., Kong, W., Wang, Z., Chang, C., and Bai, F., 2010, "Thermal Model and Thermodynamic Performance of Molten Salt Cavity Receiver," Renew. Energy, **35**(5), pp. 981–988.
[8] Palumbo, R., Venstrom, L. J., Duncan, G. S., Nudehi, S., Korenko, M., and Schoer, J., 2014, "The Solar Thermal Electrolytic Production of Mg From MgO With Concentrated Solar Energy—Quarter 2 Technical Report," Department of Energy, Advanced Research Projects Agency for Energy (ARPA-e), Washington, D.C.
[9] Thonstad, J., 2001, *Aluminium Electrolysis: Fundamentals of the Hall-Héroult Process*, 3rd ed., Aluminium-Verlag, Düsseldorf.
[10] Bergman, T. L., Incropera, F. P., DeWitt, D. P., and Lavine, A. S., 2011, *Fundamentals of Heat and Mass Transfer*, John Wiley & Sons, Hoboken, NJ.

[11] Catton, I., 1978, "Natural Convection in Enclosures," Proceedings of the International Heat Transfer Conference 6, Toronto, Canada, Aug. 7–11, 1978, pp. 13–31.
[12] Ostrach, S., 1988, "Natural Convection in Enclosures," ASME J. Heat Transfer, **110**(4b), pp. 1175–1190.
[13] Demirci, G., and Karakaya, I., 2008, "Electrolytic Magnesium Production and Its Hydrodynamics by Using an Mg–Pb Alloy Cathode," J. Alloys Compd., **465**(1–2), pp. 255–260.
[14] Holliday, R., and McIntosh, P., 1973, "Laboratory Cell and Hydrodynamic Model Studies of Magnesium Chloride Reduction in Low-Density Electrolytes," J. Electrochem. Soc., **120**(7), pp. 858–866.
[15] Korenko, M., Šimko, F., Mlynáriková, J., Larson, C., Mikšíková, E., Priščák, J., Ambrová, M., and Palumbo, R., 2019, "Physico–Chemical Properties of ($MgF_2$–$CaF_2$–$LiF)_{eut}$–MgO System as a Molten Electrolyte for Mg Electrowinning," J. Mol. Liq., **275**, pp. 535–543.
[16] Sun, Z., Cai, L., Ni, H., Lu, G.-M., and Yu, J.-G., 2018, "Coupled Electro-Thermal Field in a High Current Electrolysis Cell or Liquid Metal Batteries," R. Soc. Open Sci., **5**(2), p. 171309. (20 p.).
[17] House, J. M., Beckermann, C., and Smith, T. F., 1990, "Effect of a Centered Conducting Body on Natural Convection Heat Transfer in an Enclosure," Numer. Heat Transfer, **18**(2), pp. 213–225.
[18] Nudehi, S. S., and Venstrom, L., 2019, "Temperature Control of a Guard Heater Using Fuzzy Logic," Proceedings of the ASME 2019 Dynamic Systems and Control Conference, Park City, UT, Oct. 8–11, p. V001T02A001, 1–6.
[19] Figliola, R. S., and Beasley, D. E., 2014, *Theory and Design for Mechanical Measurements*, John Wiley & Sons, Hoboken, NJ.
[20] PTC19.1-2013, 2013, *Test Uncertainty*, ASME, New York.
[21] Globe, S., and Dropkin, D., 1959, "Natural-Convection Heat Transfer in Liquids Confined by Two Horizontal Plates and Heated From Below," ASME J. Heat Transfer, **81**(1), pp. 24–28.